A Design and Drive-Cycle Based Analysis of Direct-Driven Permanent Magnet
Synchronous Machine for a Small Urban Use Electric Vehicle

RUUSKANEN Vesa

Design and Drive-Cycle Based Analysis of Direct-Driven Permanent Magnet Synchronous Machine for a Small Urban Use Electric Vehicle

Vesa Ruuskanen[1], Janne Nerg[1], Asko Parviainen[2], Marko Rilla[3], and Juha Pyrhönen[1]
[1]LUT ENERGY, [2]AXCO-MOTORS OY, [3]VISEDO OY
Lappeenranta, Finland
Tel.: +358 / (0) – 408337959.
Fax: +358 / (0) –56212499.
E-Mail: vesa.ruuskanen@lut.fi
URL: http://www.lut.fi

Acknowledgements

Keywords

Electrical vehicle, Permanent magnet motor, Traction application

Abstract

A direct-driven permanent magnet synchronous machine for a small urban use electric vehicle is presented. The measured performance of the machine at the test bench as well as the performance over the modified New European Drive Cycle will be given. The effect of optimal current components, maximizing the efficiency and taking into account the iron loss, is compared with the simple i_d=0 – control. The machine currents and losses during the drive cycle are calculated and compared with each other.

Introduction

Environmental issues and energy efficiency are becoming more and more important aspects in modern transportation. As the greenhouse gas emissions are directly related to vehicle fuel consumption, more stringent fuel consumption standards have been set recently. Energy efficient electric and hybrid electric vehicles are one of the most attractive ways to reduce the emissions of the passenger vehicles [1] - [3].

As a hybrid electric vehicle combines a traditional propulsion system with an electrical energy storage system and an electric machine drive, the propulsion system of an electric vehicle consists only of an electric machine drive which is powered by a battery. Because the in situ emissions of an electric vehicle are zero, they can be considered as an ideal solution especially for small cars designed to urban driving cycles where the traction machine operates most frequently at light loads around the base speed, and the driving distances with one recharging being relatively short [3], [4]. In urban driving cycles the maximum speed of an electric vehicle can usually be limited to 120 km/h thus leading to much narrower speed range compared with hybrid electric vehicles. At the same time, the electric vehicle must be capable of producing high torque at low speed especially for launch and hill climbing. These aspects favor electric vehicles utilizing direct drive technology, where mechanical gear is replaced by an electrical one thus reducing the total weight of the vehicle.

The research in the field of electrical traction drives has been quite intense during the past decade. The usability of several electrical machine types for electrical vehicles has been studied. According the

A Design and Drive-Cycle Based Analysis of Direct-Driven Permanent Magnet
Synchronous Machine for a Small Urban Use Electric Vehicle

RUUSKANEN Vesa

results found e.g. in [4] - [10], the most popular electric machine type for vehicles is permanent magnet synchronous machine (PMSM). The main advantages of PMSMs are the high electrical efficiency and highest torque density of the present day electrical machines leading to the lightest possible construction. PMSMs are also well suitable for direct-driven applications. Furthermore, by selecting a machine topology where permanent magnets are embedded inside the rotor structure the magnets are effectively shielded from the demagnetizing armature reaction field. The negative saliency of the magnetic circuit also allows the utilization of reluctance torque.

In traction applications, both the speed and torque of the machine change almost continuously between zero and the maximal value. Therefore, the machine performance must be studied over the drive cycle of the vehicle instead of in the rated operating point of the machine only. In literature, it is suggested that the New European Driving Cycle performance of the PMSM can be determined with a sufficient accuracy based on a set of only twelve characteristic points in which the machine is analyzed to reduce computational time [11, 12]. The comparison of different machine types over the New European Driving Cycle using time transient Finite Element Analysis is carried out in [13].

In this paper a PMSM for a small, urban use electric vehicle is presented. The machine comprises of an integer wound stator and a rotor where two layers of shaped Neodymium-Iron-Boron (NeFeB) permanent magnets are embedded inside the laminated rotor structure. It is shown that the proposed PMSM is capable of enhanced reluctance torque production capability. The New European Driving Cycle performance of the designed machine is analyzed using the drive cycle simulation tool based on the magnetostatic FEA. The practical measurements demonstrating the machine performance are also given.

Design specification

The electric vehicle to be considered is a rear wheel driven and it utilizes two direct-driven PMSMs. For this application, the dimensional envelope of the PMSM, set by the industrial partner, requires a radial flux machine with a maximum stator external diameter of 300 mm and a maximum active length (including active stack and end-windings) of 260 mm. The maximum speed of the electric vehicle is set to 120 km/h and due to the wheel diameter of 0.62 m, it occurs at 1077 rpm. The battery voltage is 350 V corresponding maximum root-mean-square (RMS) line-to-line voltage of 247 V. The nominal power of one PMSM is 20 kW and the nominal speed is set to 1200 rpm. Therefore, the nominal torque is 160 Nm. It must be noticed that in this application no field weakening is required during normal operation.

In the machine design, a rotor construction where two layers of shaped NdFeB-magnets are embedded inside the laminated rotor structure was selected as a base solution. Similar rotor construction was used by the authors in the traction motors of full electric sports car Electric RaceAbout [14]. The stator winding type was selected to be a two layer integral slot winding.

Because the PMSM is totally enclosed structure, the stator frame is liquid cooled in such a way that there are spiral cooling fluid flow channels in the outer surface of the stator frame. The tangential stress for the machine was selected to σ_{Ftan} = 21 kPa leading to the rotor outer diameter of 210 mm and an active stack length of 110 mm. The torque-per-unit-rotor-volume (TRV) is 42 kNm/m^3. The electrical steel lamination used both in the stator and rotor stacks was M400-50A. In order to minimize the end effects and the resulting loss in the no-load voltage, the rotor stack is made 4 mm longer than the stator stack [15], [16]. As the number of pole pairs affect directly to the required stator yoke height, the number of pole pairs was selected to be 7, thus leading to the structure where the maximum stator external diameter was not exceeded. The air gap length in direct-axis was selected to 1.3 mm and the rotor pole structure was shaped in such a way that the quadrature axis air gap maximum value is 4.3 mm. In order to reduce cogging torque and load torque ripple the stator stack was skewed one stator slot pitch. Structure of the designed PMSM is depicted in Fig. 1 and the main parameters of the PMSM are presented in Table 1.
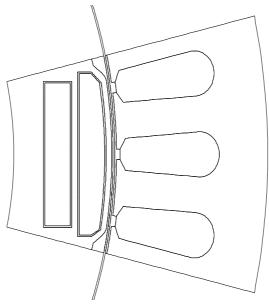
Fig. 1: Schematic of one pole of the designed PMSM

Table I: Main parameters of the designed PMSM

Number of pole pairs	7
Number of phases	3
Number of stator slots	42
Stator outer diameter	298 mm
Stator bore diameter	212.6 mm
Active stator stack length	110 mm
Active rotor stack length	114 mm
Rotor outer diameter	210 mm
Air-gap length (min)	1.3 mm
Permanent magnet type	Neorem 753a
Length of the upper magnet	38.5 mm
Length of the lower magnet	34 mm
Thickness of the upper magnet	7.1 mm
Thickness of the lower magnet	7 mm
Number of slots per pole per phase	1
Number of conductor in one slot	10

A Design and Drive-Cycle Based Analysis of Direct-Driven Permanent Magnet
Synchronous Machine for a Small Urban Use Electric Vehicle
RUUSKANEN Vesa

Number of conductor in series per phase	70
Stator winding connection	star
Rated line to line voltage	240 V
Rated speed	1200 rpm
Rated phase current	56 A
Rated frequency	140 Hz
Rated power	20 kW

Numerical results

The performance characteristics of the designed PMSM were evaluated using two-dimensional finite element method. To take the skewing into account in the FE-analysis the no-load and load torque ripple calculations were done with the skew-module of Flux2D/3D-software package. All the transient calculations are performed with non-linear time-stepping scheme. In the synchronous inductance and the torque component calculations, the frozen permeability method was applied to form additional linear solutions.

The calculated phase and line-to-line no-load voltages as a function of time at the rotational speed of 1200 rpm are presented in Fig. 2. The reason why the measured line no-load voltage is slightly higher than the calculated value is because the longer rotor stack, which in this case completely compensated the end effects.
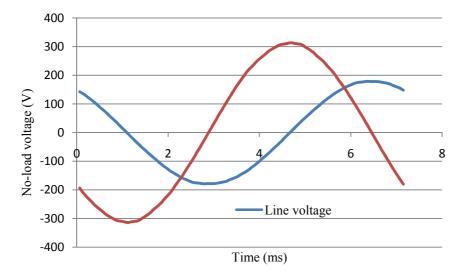

Fig. 2: Calculated phase and phase-to-phase no-load voltages at the speed of 1200 rpm. The calculation has been performed at magnet temperature of 20 ºC corresponding remanence flux density of 1.28 T. The calculated RMS value of the phase no-load voltage is 128.0 V and the measured no-load voltage is 128.8 V.

In order to separate the total torque to excitation and reluctance components, the frozen permeability method has to be applied [17]-[19]. The calculation has been done as follows: For each load angle the instantaneous phase currents and angular position are recorded over one pole pair from the stable transient solution. These values are used to formulate a set of static solutions, one for each angular position. Static problem with a given angular position and phase currents is solved. Then the

reluctances in each element of the finite element mesh are recorded and used in a new static problem, which uses the same phase currents but the magnets are switched off, that is, they are replaced with a material having the relative permeability of 1.05 and remanence flux density of 0 T. The torque computed from these static problems corresponds to the reluctance torque. For every load angle the reluctance torque is computed as an average value over one pole pair. The reason why the calculation is extended over one pole pair is to take the magnetic circuit variation into account. The calculated torque components as a function of the load angle for the designed PMSM are shown in Fig. 3.
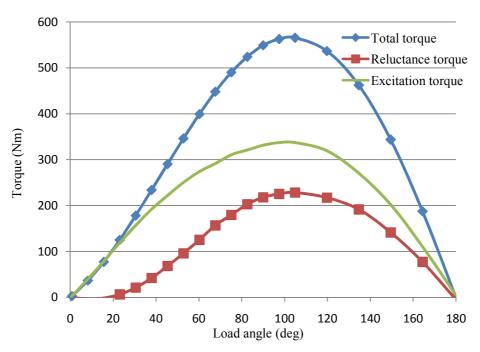

Fig. 3: Calculated torque components as a function of the load angle

As we can see from Fig. 3, the reluctance torque is negligible at low load angles, but at the load angle operation range of 50 – 105 electrical degrees the reluctance torque is significant, that is a 2/3 of the excitation torque. According to the calculation result, the design succeeded in its aim to maximize reluctance torque production capability.

For a proper PMSM control, the PMSM synchronous inductances must be known as accurately as possible over the whole operation range of the machine. In order to take the cross-saturation between the d- and q-axes into account in the synchronous inductance calculation, the PMSM synchronous inductances were calculated at locked-rotor position for different sets of direct- and quadrature-axis currents (i_d and i_q) by a static two-dimensional FEM. The direct- and quadrature-axis flux linkages ψ_d and ψ_q were calculated for each i_d and i_q combination from phase flux linkages utilizing Park transformation. Cross saturated incremental values for synchronous inductances L_d and L_q are calculated as

$$L_d = \left.\frac{\Delta\Psi_d}{\Delta i_d}\right|_{i_q=\text{constant}} , \tag{1}$$

$$L_q = \left.\frac{\Delta\Psi_q}{\Delta i_q}\right|_{i_d=\text{constant}} , \tag{2}$$

where the change of current components (Δi_d and Δi_q) is kept very small. The calculated d- and q-axis synchronous inductances as a function of the d- and q-axis currents are shown in Fig. 4 and Fig. 5.
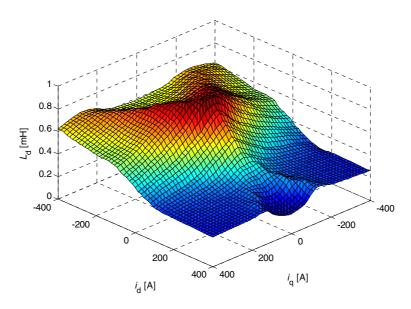
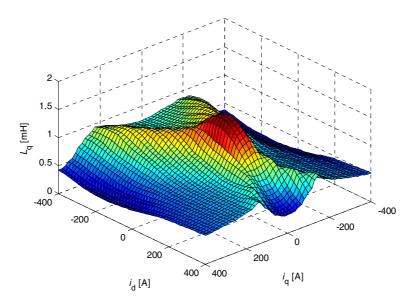Fig. 4: Incremental value of the direct-axis synchronous inductance

Fig. 5: Incremental value of the quadrature-axis synchronous inductance

It can be seen that the value of the dynamic synchronous inductance varies dramatically as a function of current components. Heavy saturation can be caused by any positive direct-axis current or armature reaction caused by high quadrature-axis current component amplitude. During normal operation field intensifying positive d-axis current is not used, but high q-axis current values exist when high torque is produced. The q-axis inductance varies more than the d-axis inductance as a function of currents, because the permanent magnets affect q-axis inductance only by means of cross-saturation. To reach high accuracy the machine saturation must be taken into account during the drive cycle analysis also and analysis with constant parameters would lead to erroneous results.

Experimental results

In the measurements the PMSM was driven by ABB's ACSM1 frequency converter. The test setup consisted of a 500 kW three phase induction machine, Magtroll 2000 Nm torque meter, and Yokogawa PZ-4000 power analyzer. The designed PMSM in test bench is shown in Fig. 6.
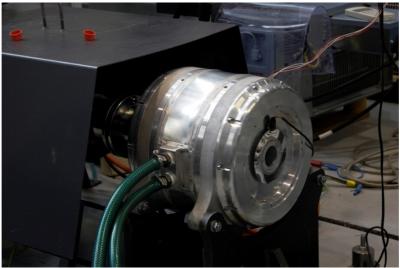

Fig. 6: Designed PMSM in test bench

The measured phase no-load voltage was 128.8 V at the rotational speed of 1200 rpm. The on-load testing was done at the rotational speed of 1077 rpm. The motor torque was 177 Nm corresponding to the output power of 20 kW. The motor was cooled with water the inlet temperature of which was 15 ºC and the volumetric flow rate was 0.3 m^3/h. The steady state temperature of the stator coils measured with Pt100 temperature sensors was 75 ºC. The measured efficiency was 96 % and the power factor for the fundamental wave was 0.96.

Drive cycle analysis

The drive cycle is a simplified version of New European Driving Cycle (NEDC). The NECD includes urban and extra-urban parts. During the urban part the Urban Driving Cycle (ECE 15) with duration of 195 s is repeated four times. The Extra Urban Driving Cycle (EUDC) with durations of 400 s is driven only once. In this paper, the urban driving cycle is repeated just once instead of four times in NEDC leading to the total duration of 595 s. To see the effect of field weakening, the maximum value of the line-to-line voltage is set to 350 V and the speed of NEDC is multiplied by 3/2 increasing the maximum speed from 120 km/h to 180 km/h although it is well above the desired operating area. The rotational speed of the machine during the selected drive cycle is shown in Fig. 7.
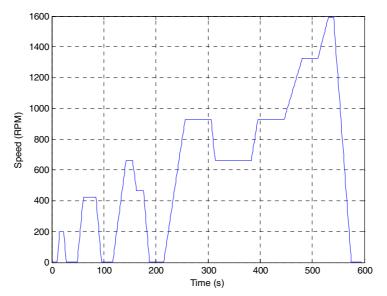
Fig. 7: Rotational speed of the direct-driven motor during the drive cycle. The rated top speed 120 km/h equals 1077 rpm with 0.62 m wheel diameter.

The drive cycle analysis is based on the flux linkage values calculated with 2D FEA as a function of current components. The iron loss at no load is calculated using the LS-model of the Flux2D-software. The iron loss during the drive cycle is assumed to be directly proportional to the back electromotive force of the machine and determined based on the no-load FEA. Two variations of the machine current components during the drive cycle are analyzed. First of all, the i_d=0 –control is applied by setting the direct-axis current to zero and finding the minimum quadrature-axis current producing the desired torque. In the second case, the optimal current components are found maximizing the efficiency including the effect of iron loss. The total torque and the reluctance torque components are shown in Fig. 8.
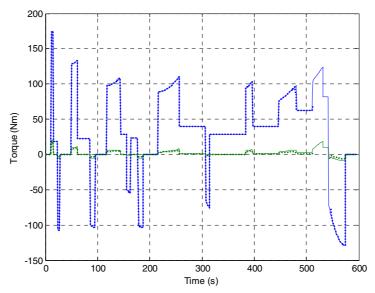

Fig. 8: Total torque (blue) and the reluctance torque (green) during the drive cycle. The dashed line presents the i_d=0 -variation and the solid line the maximal efficiency variation.

The total torque is obviously same for both variations except during the highest speeds, way over the designed top speed of the vehicle, where i_d=0 -control cannot be used because the voltage limit is reached. The reluctance torque is relatively small because the machine does not operate deep in the

field weakening region and the torque needed is small compared with the torque capability of the machine leading to a small load angle. The current components are shown in Fig. 9.
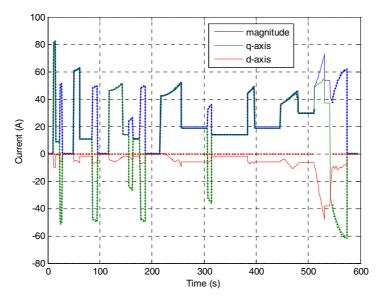

Fig. 9: Current components and current magnitude during the drive cycle. The dashed line presents the i_d=0 -variation and the solid line the maximal efficiency variation.

The q-axis current components differ from each other only slightly, because q-axis current is the main torque producing current component. Demagnetizing negative d-axis current is used during high speed periods to decrease the iron loss and limit the stator voltage. The copper and iron loss components are shown in Fig. 10.
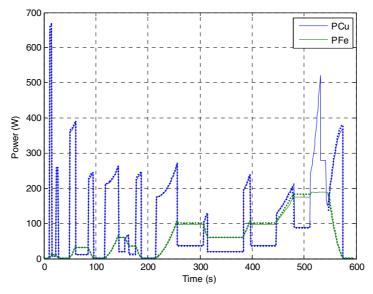

Fig. 10: Copper and iron loss components during the drive cycle. The dashed line presents the i_d=0-variation and solid line the maximal efficiency variation.

The difference in copper loss is very small. The iron loss with the optimal current components is slightly smaller than with i_d=0 -control during the highest rotational speeds. Because of the relatively low synchronous inductance values the demagnetizing negative d-axis current cannot be used to significantly reduce iron loss during the cycle without increase of copper loss. The difference in total loss is not significant between studied control methods and also i_d=0 -control offers high effciency when the stator voltage limit is not reached.

A Design and Drive-Cycle Based Analysis of Direct-Driven Permanent Magnet
Synchronous Machine for a Small Urban Use Electric Vehicle

RUUSKANEN Vesa

Conclusion

The design process of a direct-driven PMSM for a small urban use electric vehicle was presented. The performance characteristics of the designed PMSM were calculated utilizing two-dimensional finite-element-analysis. The calculation results were compared with the practical measurements and a good correlation was found. At the nominal speed and torque the measured efficiency was 96 %. The behavior of the PMSM was analyzed over the drive cycle based on the New European Driving Cycle. The performances using the i_d=0 -control and the optimal current components maximizing the efficiency were compared with each other.

References

[1] C. C. Chan: The State of the Art of Electric and Hybrid Vehicles, Proc. IEEE Vol. 90 no 2, pp. 247-275

[2] K. T. Chau, C. C. Chan, C. Liu: Overview of Permanent-Magnet Brushless Drives for Electric and Hybrid Electric Vehicles, IEEE Trans. Ind. Electron. Vol. 55 no 6, pp. 2246-2257

[3] C. C. Chan, A. Bouscayrol, K. Chen: Electric, Hybrid, and Fuel-Cell Vehicles: Architectures and Modeling, IEEE Trans. Veh. Technol. Vol. 59 no 2, pp. 589-598

[4] Z. Q. Zhu, D. Howe: Electrical Machines and Drives for Electric, Hybrid, and Fuel Cell Vehicles, Proc. IEEE Vol. 95 no 4, pp. 746-765

[5] D. G. Dorrell, A. M. Knight, M. Popescu: Performance Improvement in High-Performance Brushless Rare-Earth Magnet Motors for Hybrid Vehicles by Use of High Flux-Density Steel, IEEE Trans. Magn. Vol. 47 no 10, pp. 3016-3019

[6] A. Wang, Y. Jia, W. L. Soomg: Comparison of Five Topologies for an Interior Permanent-Magnet Machine for a Hybrid Electric Vehicle, IEEE Trans. Magn. Vol. 47 no 10, pp. 3606-3609

[7] G. Pellegrino, A. Vagati, P. Guglielmi, B. Boazzo: Performance Comparison Between Surface-Mounted and Interior PM Motor Drives for Electric Vehicle Application, IEEE Trans. Ind. Electron. Vol. 59 no 2, pp. 803-811

[8] P. H. Nguyen, E. Hoang, M. Gabsi: Performance Synthesis of Permanent-Magnet Synchronous Machines During the Driving Cycle of a Hybrid Electric Vehicle, IEEE Trans. Veh. Technol. Vol. 60 no 5, pp. 1991-1998

[9] K. I. Laskaris, A. G. Kladas: Internal Permanent Magnet Motor Design for Electric Vehicle Drive, IEEE Trans. Ind. Electron. Vol. 57 no 1, pp. 138-145

[10] A. EL-Refaie: Fractional-Slot Concentrated-Windings Synchronous Permanent Magnet Machines: Opportunities and Challenges, IEEE Trans. Ind. Electron. Vol. 57 no 1, pp. 107-121

[11] P. Lazari, J. Wang, and L. Chen: A computationally efficient design technique for electric vehicle traction machines, Proc. 20th Int. Conf. on Elect. Mach. (ICEM '12), Marseille, France, Sep. 2012, pp. 2596–2602.

[12] L. Chen, J. Wang, P. Lombard, P. Lazari, and V. Leconte: Design optimization of permanent magnet assisted synchronous reluctance machines for electric vehicle applications, Proc. of the 20th International Conference on Electrical Machines, ICEM 2012, Marseille, France, Sep. 2012, pp. 2647–2653.

[13] G. Pellegrino, A. Vagati, B. Boazzo, and P. Guglielmi: Comparison of induction and PM synchronous motor drives for EV application including design examples, IEEE Trans. Ind. Appl. Vol. 48 no 6, pp. 2322–2332

[14] J. Nerg, M. Rilla, V. Ruuskanen, J. Pyrhönen, and S. Ruotsalainen: Direct-driven interior magnet permanent magnet synchronous motors for a full electric sports car, IEEE Trans. Ind. Electron. Vol. 61 no 8, pp. 4286-4294

[15] J. Pyrhönen, V. Ruuskanen, J. Nerg, J. Puranen, H. Jussila: Permanent-Magnet Length Effects in AC Machines, IEEE Trans. Magn. Vol. 46 no 10, pp. 3783-3789

[16] V. Ruuskanen, J. Nerg, J. Pyrhönen: Effect of Lamination Stack Ends and Radial Cooling Channels on No-Load Voltage and Inductances of Permanent-Magnet Synchronous machines, IEEE Trans. Magn. Vol. 47 no 11, pp. 4643-4649

[17] N. Bianchi, S. Bolognani: Magnetic models of saturated interior permanent magnet motors based on finite element analysis, n Proc. 33rd IAS Annu. Meeting, October 1998, St. Louis, Missouri, USA, pp. 27-34.

[18] J. A. Walker, D. G. Dorrell, C. Cossar: Flux-Linkage Calculation in Permanent-Magnet Motors Using the Frozen Permeabilities Method, IEEE Trans. Magn. Vol 41 no 10, pp. 3946-3948

[19] D. G. Dorrell, M-F. Hsieh, M. Popescu, L. Evans, D. A. Staton, V. Grout: A Review of the Design Issues and Techniques for Radial-Flux brushless Surface and Internal Rare-Earth Permanent-Magnet Motors, IEEE Trans. Ind. Electron. Vol. 58 no 9, pp. 3741-3756